RADIO PLASMA IMAGER SIMULATIONS AND MEASUREMENTS

J. L. GREEN[1], R. F. BENSON[1], S. F. FUNG[1], W. W. L. TAYLOR[2], S. A. BOARDSEN[2], B. W. REINISCH[3], D. M. HAINES[3], K. BIBL[3], G. CHENEY[3], I. A. GALKIN[3], X. HUANG[3], S. H. MYERS[3], G. S. SALES[3], J.-L. BOUGERET[4], R. MANNING[4], N. MEYER-VERNET[4], M. MONCUQUET[4], D. L. CARPENTER[5], D. L. GALLAGHER[6] and P. H. REIFF[7]

[1]*NASA Goddard Space Flight Center, U.S.A.*
[2]*Raytheon Corporation, NASA Goddard Space Flight Center, Greenbelt, MD, U.S.A.*
[3]*University of Massachusetts, Center for Atmospheric Research, Lowell, MA, U.S.A.*
[4]*Observatoire de Paris, Meudon, France*
[5]*Stanford University, Stanford, CA, U.S.A.*
[6]*NASA Marshall Space Flight Center, Huntsville, AL, U.S.A.*
[7]*Rice University, Houston, TX, U.S.A.*

(Received May 7, 1999)

Abstract. The Radio Plasma Imager (RPI) will be the first-of-its kind instrument designed to use radio wave sounding techniques to perform repetitive remote sensing measurements of electron number density (N_e) structures and the dynamics of the magnetosphere and plasmasphere. RPI will fly on the Imager for Magnetopause-to-Aurora Global Exploration (IMAGE) mission to be launched early in the year 2000. The design of the RPI is based on recent advances in radio transmitter and receiver design and modern digital processing techniques perfected for ground-based ionospheric sounding over the last two decades. Free-space electromagnetic waves transmitted by the RPI located in the low-density magnetospheric cavity will be reflected at distant plasma cutoffs. The location and characteristics of the plasma at those remote reflection points can then be derived from measurements of the echo amplitude, phase, delay time, frequency, polarization, Doppler shift, and echo direction. The 500 m tip-to-tip X and Y (spin plane) antennas and 20 m Z axis antenna on RPI will be used to measures echoes coming from distances of several R_E. RPI will operate at frequencies between 3 kHz to 3 MHz and will provide quantitative N_e values from 10^{-1} to 10^5 cm^{-3}. Ray tracing calculations, combined with specific radio imager instrument characteristics, enables simulations of RPI measurements. These simulations have been performed throughout an IMAGE orbit and under different model magnetospheric conditions. They dramatically show that radio sounding can be used quite successfully to measure a wealth of magnetospheric phenomena such as magnetopause boundary motions and plasmapause dynamics. The radio imaging technique will provide a truly exciting opportunity to study global magnetospheric dynamics in a way that was never before possible.

1. Introduction

Unlike a traditional *in situ* magnetospheric instrument, RPI's main purpose is to generate radio waves that travel great distances in the magnetosphere, reflect within magnetospheric plasmas, and then receive and measure the characteristics of the reflected waves or echoes. The wave frequency of the echoes provides detailed information about the remote plasma density and motion. One of RPI's fundamental

Space Science Reviews **91:** 361–389, 2000.

measurements is the time between wave emission and the reception of the echo. From the time delays of a sequence of echoes at stepped frequencies, an accurate distance to the remote plasma region can be determined. The three-axis antenna system RPI uses will enable the instrument to measure the echo direction of arrival. In addition, RPI will also stimulate the local plasma environment providing much valuable *in situ* measures. The design of the RPI is described elsewhere in this monograph (Reinisch et al., 2000).

Extensive ray tracing calculations have been performed over the last several years by Reiff et al. (1994), Fung and Green (1996), Reiff et al. (1996), Green et al. (1996, 1998a,b) and Benson et al. (1998b). These simulations provide a roadmap for understanding the resulting echo spectrum of the magnetosphere and clearly show the new results that can be obtained along with the limitations of the instrument. In the following sections we will discuss the basic principle of radio sounding, provide an overview of the results of ray tracing simulations, review RPI's ability to make *in situ* measurements, and discuss the expected results.

2. Basic Principles

It is well known that there are two modes of free-space electromagnetic waves propagating in a cold plasma at frequencies greater than the electron plasma frequency (see, for example, Stix, 1962). The term free-space wave mode is used to describe an electromagnetic wave that propagates freely in a tenuous plasma as if it were in a vacuum. These waves will only alter their direction when significant changes in the medium occur. The two free-space wave modes are the left-hand ordinary (L-O or just O) and the right-hand extra-ordinary (R-X or just X).

A wave's cutoff frequency within a plasma is the location where the index of refraction tends to zero and complete reflection occurs. The O mode wave cutoff is equal to the ambient electron plasma frequency or f_p, which is related to the electron number density N_e and is given by:

$$f_{\mathrm{LO}} = f_p \cong 9\sqrt{N_e} \tag{1}$$

where f_p is expressed in Hz and N_e in m^{-3} (or kHz and cm^{-3}, respectively).

The X mode wave cutoff depends on the ambient f_p and the electron gyrofrequency (f_g) and is given by:

$$f_{\mathrm{RX}} = \frac{f_g}{2} + \left[\left(\frac{f_g}{2}\right)^2 + f_p^2\right]^{1/2} . \tag{2}$$

For a space plasma sounder to operate properly, it must generate short-duration radio wavelength electromagnetic pulses in the O and/or X modes. Once generated, these waves will travel undisturbed until the wave approaches a plasma cutoff where it will then suffer a refraction or reflection. A reflection occurs in a region of

space where the transmitted radio wave frequency equals the local plasma cutoff, since the refractive index for that mode then goes to zero.

The radio sounder receiver detects an echo when sounder-generated waves return to the instrument after encountering its distant wave-cutoff frequency. More complicated multiple reflections can occur that do produce echoes, however, these are not expected to be typical. The sounder will measure a number of attributes of the echo along with the time from transmission to reception called the delay or echo time. As can be seen from Equation (1), radio sounding in the O mode can be used to obtain accurate remote N_e measurements in magnetized space plasmas.

Ionospheric sounding using ground-based ionosondes has been carried out for seven decades using the radio sounding technique (Breit and Tuve, 1926). Since this sounding is based on total reflection, only those signals reflected between the sounder and the location of the peak f_p (typically 300 km) can be returned during vertical-sounding experiments.

Ionospheric radio sounders placed on satellites (known as topside sounders) have been used to remotely investigate the region from the altitude of the spacecraft down to the altitude of the ionospheric peak (Jackson et al., 1980; Jackson, 1986). The shielding effect of the ionosphere prevents routine ground-based sounding of the magnetosphere. The RPI instrument on IMAGE is designed to perform repetitive remote sensing measurements of N_e structures and deduce the dynamics of the magnetosphere and plasmasphere by using radio sounding techniques.

3. Radio Sounder Measurements

IMAGE will be launched into a highly elliptical polar orbit with an apogee geocentric distance of 8 R_E (the mean Earth radius, R_E, is 6371 km). Its prime mission will be of two years' duration with one additional year of data analysis. During the prime mission the IMAGE orbit apogee will precess over the north pole as illustrated in Figure 1. During most of its prime operation, the apogee of IMAGE will be above 45° north geographic latitude. In this region, the spacecraft will be in the magnetospheric N_e cavity extending from the plasmapause to the magnetopause. When in the magnetospheric N_e cavity, RPI will be able to simultaneously receive echoes from the magnetopause and the plasmapause. RPI is called an imager rather than a sounder because, in addition to measuring echo signal strength and delay time as a function of sounding frequency, it will be capable of measuring the echo direction-of-arrival and Doppler spectrum in order to produce 'echo maps' of the echoing structures (Reinisch et al., 1999). The 500 m tip-to-tip X and Y (spin plane) dipole antennas and 20 m tip-to-tip Z axis dipole antenna on RPI will be used to measure the direction of arrival of the echoes coming from distances of many R_E (Reinisch et al., 1999). RPI will operate at frequencies between 3 kHz to 3 MHz and will provide quantitative N_e values from 10^{-1} to 10^5 cm^{-3} with high precision.

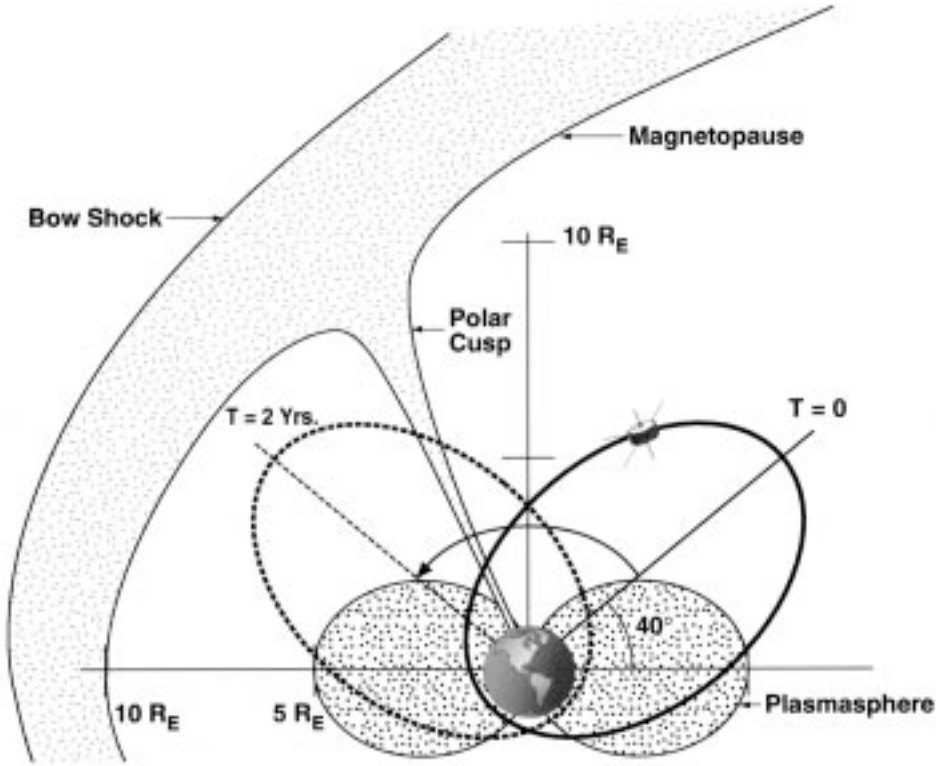

Figure 1. Schematic illustration of the IMAGE spacecraft orbit in the magnetosphere. The magnetospheric N_e cavity extends from the plasmapause to the magnetopause. The RPI on IMAGE will be able to simultaneously perform radio sounding upward toward the magnetopause and downward toward the plasmapause.

An obvious difference between ionospheric and magnetospheric sounding is in the distances or ranges involved between the sounder and the reflecting medium. In the ionosphere, the range is on the order of hundreds to thousands of km; in the magnetosphere, the range will be many R_E, i.e., greater by several factors of 10. Another difference is that the assumption that the medium is horizontally stratified holds in most situations of ionospheric sounding but not in the case of magnetospheric sounding. The magnetosphere presents curved targets for a sounder located between the plasmapause and the magnetopause. In this situation the plasmapause is a convex target which when sufficiently 'smooth' causes a slightly decreased echo power return due to defocusing, whereas the magnetopause is a concave target which yields a slightly increased echo power return due to focusing. As shown in the calculations by Calvert et al., (1995), the change in power is approximately 2.5 for both the magnetopause and for the plasmapause when compare with echoes from a flat surface. Decreased power return from the plasmapause due to defocusing does not pose a problem for RPI on IMAGE because the antenna

system will operate at its greatest efficiency within the plasmapause sounding frequency range. The increased echo power due to focusing at the magnetopause is helpful because the low electron density there requires sounding frequencies that will be well below 100 kHz most of the time. In this frequency range the transmitted power is proportional to f^4 and even the long 500-m dipoles are very inefficient radiators at such low frequencies (Calvert et al., 1995). Under normal conditions it is expected that RPI will be able to detect magnetopause echoes within a distance of approximately 4 R_E.

3.1. RAY TRACING SIMULATIONS

Ray tracing calculations have been performed to simulate the return pulses or echoes from RPI transmissions on IMAGE located in a model magnetosphere. The first formulation of ray-tracing equations that were suitable for integration by standard numerical methods using computers was done in the mid-1950s by Haselgrove. Haselgrove (1955) developed six first-order differential equations that describe the motion of the energy in electromagnetic waves propagating in an anisotropic medium in three dimensions. These equations are:

$$\frac{\mathrm{d}r}{\mathrm{d}t} = \frac{1}{N^2}\left(n_r - N\frac{\partial N}{\partial n_r}\right) , \tag{3}$$

$$\frac{\mathrm{d}\theta}{\mathrm{d}t} = \frac{1}{rN^2}\left(n_\theta - N\frac{\partial N}{\partial n_\theta}\right) , \tag{4}$$

$$\frac{\mathrm{d}\phi}{\mathrm{d}t} = \frac{1}{rN^2\sin\theta}\left(n_\phi - N\frac{\partial N}{\partial n_\phi}\right) , \tag{5}$$

$$\frac{\mathrm{d}n_r}{\mathrm{d}t} = \frac{1}{N}\left(\frac{\partial N}{\partial r} + n_\theta\frac{\mathrm{d}\theta}{\mathrm{d}t} + n_\phi\frac{\mathrm{d}\phi}{\mathrm{d}t}\sin\theta\right) , \tag{6}$$

$$\frac{\mathrm{d}n_\theta}{\mathrm{d}t} = \frac{1}{r}\left(\frac{1}{N}\frac{\partial N}{\partial\theta} - n_\theta\frac{\mathrm{d}r}{\mathrm{d}t} + rn_\phi\frac{\mathrm{d}\phi}{\mathrm{d}t}\cos\theta\right) , \tag{7}$$

$$\frac{\mathrm{d}n_\phi}{\mathrm{d}t} = \frac{1}{r\sin\theta}\left(\frac{1}{N}\frac{\partial N}{\partial\phi} - n_\phi\frac{\mathrm{d}r}{\mathrm{d}t}\sin\theta - rn_\phi\frac{\mathrm{d}\theta}{\mathrm{d}t}\cos\theta\right) , \tag{8}$$

where the index of refraction is:

$$N^2 = n_r^2 + n_\theta^2 + n_\phi^2 .$$

Equations (3), (4), and (5) describe the time rate of change in the position of a ray. Equations (6), (7), and (8) describe the time rate of change of the components of the index of refraction (N) with respect to the ray position (r, θ and ϕ). These equations express the motion of the energy of the wave in spherical coordinates.

The above ray tracing equations of Haselgrove allowed for the inclusion of one of many formulations for N. The expression for N used in the RPI simulations is for radiation in a cold plasma that has been developed by Stix (1962). This expression is:

$$N^2 = \frac{[RL\ \sin^2\theta + PS(1+\cos^2\theta)] \pm [(RL - PS)^2 \sin^2\theta + 4P^2D^2\cos^2\theta]}{(S\ \sin^2\theta + P\ \cos^2\theta)}\ , \tag{9}$$

where

$$R = 1 - \sum_s \frac{f_{ps}^2}{f(f + f_{gs})}\ , \tag{10}$$

$$L = 1 - \sum_s \frac{f_{ps}^2}{f(f - f_{gs})}\ , \tag{11}$$

$$P = 1 - \sum_s \frac{f_{ps}}{f^2}\ , \tag{12}$$

$$S = \tfrac{1}{2}(R + L)\ , \tag{13}$$

$$D = \tfrac{1}{2}(R - L)\ . \tag{14}$$

A cold plasma formulation of N requires immobile electrons and ions relative to the velocity of the ray and does not take into account any hot plasma effects. Since the velocity of rays traveling in the free space mode is almost always near the speed of light, the index of refraction based on cold plasma is completely appropriate.

In order to obtain realistic echoes, the plasma and magnetic field models that are used in the ray tracing code must be acceptable representations of the physical environment that influences the radiation. The magnetic field model employed in the ray tracing simulations is a simple dipole model, while the plasma density model is a combination of models of diffusive equilibrium by Angerami and Thomas (1964), of the ionosphere and plasmasphere by Kimura (1966), of the plasmapause by Aikyo and Ondoh (1971) and of the magnetopause by Roelof and Sibeck (1993).

3.2. PLASMAGRAMS

The primary presentation of RPI data will be in the form of plasmagrams, which are the magnetospheric analogs of ionograms. A plasmagram is a plot of echo power as a function of frequency and echo delay. Simulated magnetospheric X- and O-mode echoes, as anticipated to be received by RPI and derived from ray tracing calculations, are presented in Figure 2. The RPI simulated echoes are presented in the form of echo time delay (t), expressed in terms of apparent range (left scale), as

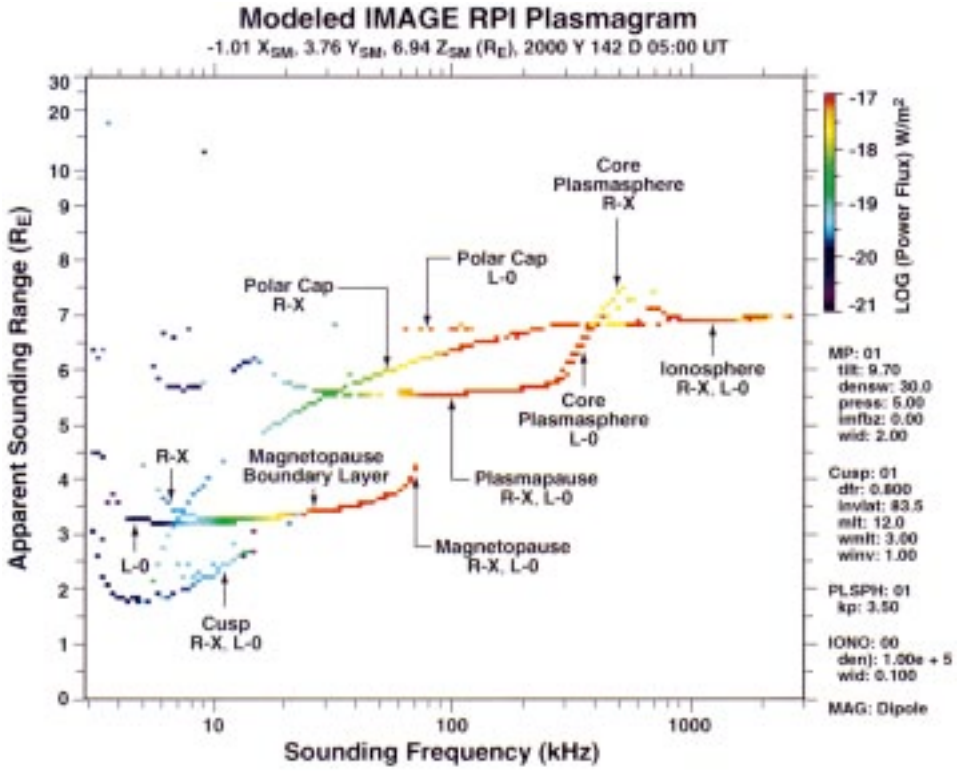

Figure 2. A simulated plasmagram illustrating the structure of the echoes anticipated from a routine sounding by RPI when IMAGE is near apogee.

a function of the sounder frequency (bottom scale). The apparent range corresponds to $ct/2$ where c is the speed of light. The intensity is color-coded and has been calculated for each echo in this figure. The location of the spacecraft for this simulation is at approximately 19 hours magnetic local time near apogee (approximately 8 R_E) at about 60° magnetic latitude. The simulated echoes in the plasmagram of Figure 2 are labeled with their appropriate propagation modes (R-X, L-O) and regions in the magnetosphere in which the echoes have occurred (i.e., the plasmasphere, plasmapause, magnetopause, polar cap, and polar cusp). The plasmagram contains the simulated echo measurements from a complete RPI instrument cycle when the spacecraft is near apogee. A complete RPI instrument cycle (transmission plus echo reception) typically takes several minutes to complete. As can be seen the resulting plasmagram can be quite complicated with echoes from several regions over an extended frequency range and a wide range of distances.

In order to reduce the complexity of the plasmagram of Figure 2 and to illustrate how these echoes are used in the analysis of magnetospheric density structures and motions, simulated echoes from the magnetopause boundary layer have been isolated and shown in Figure 3. Panels B and D on the right, in Figure 3, show two

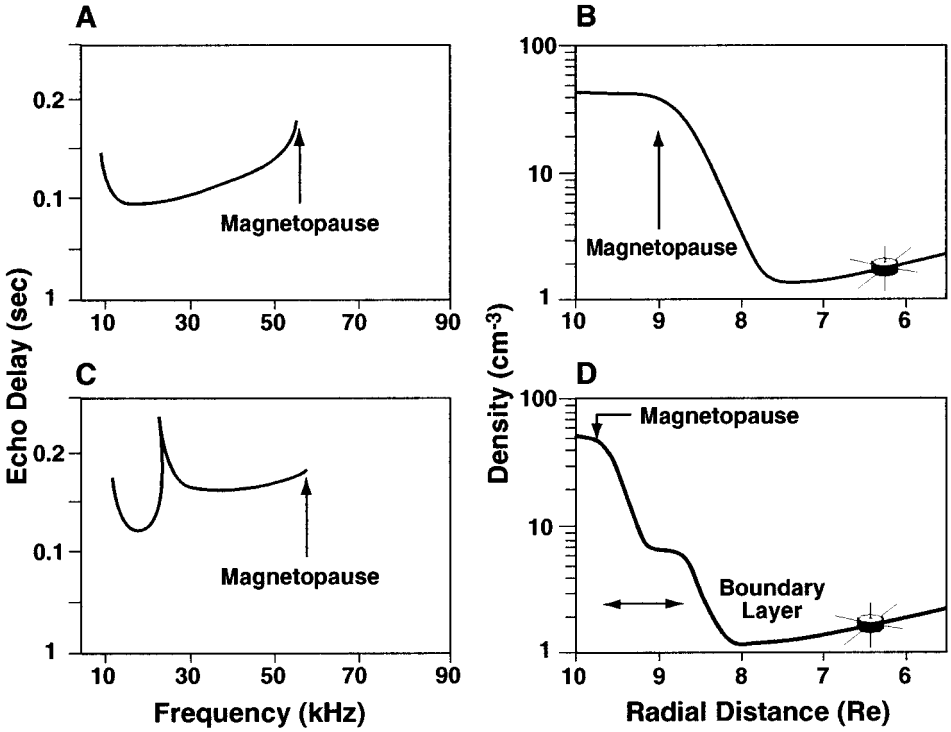

Figure 3. Two representative magnetopause boundary layers (A and C) and the corresponding density structures (B and D).

distinct density profiles which may occur in the boundary layer and magnetopause under different solar wind and interplanetary magnetic field conditions. The spacecraft in panels B and D show the location of the RPI relative to these density structures. The two left-hand panels, A and C in Figure 3, depict the corresponding simulated plasmagrams. For comparison, the echo structure of the magnetopause boundary layer in the upper left panel of Figure 3 can easily be seen in Figure 2.

The plasmagrams of Figure 3 (panels A and C) have echoes that start at a large apparent range because the transmitted wave going toward the magnetopause initially propagates into a region of decreasing N_e and must travel some distance before encountering an N_e value capable of causing total reflection. The delay time then decreases with increasing frequency for a short frequency interval, even though the wave is penetrating deeper into the medium, because the wave propagation speed increases as the frequency increases. When the frequency of the sounder exceeds the maximum plasma frequency at the magnetopause, the echo trace stops. The additional density in the boundary layer structure of panel D has the effect of slowing down (increasing delay time) the echoes at the lower frequencies causing a 'cusp' like structure in the corresponding plasmagram of panel C. Panels A and

C show that the two echo traces are significantly different and that the echo traces are sensitive indicators of the density structures involved in the reflection.

As in the case of ionospheric topside-sounders, the N_e profiles from RPI will be deduced from the reflection traces (Figure 2, panels A and C of Figure 3) using the standard inversion techniques developed by Jackson (1969) and Huang and Reinisch (1982). This technique has been applied to a number of echoes of the simulated plasmagrams and the resulting density profiles are nearly identical to those used in the ray tracing calculations. In addition to deriving N_e profiles, it will be possible to construct N_e contours in the orbital plane as was done using ionospheric topside sounding (see, e.g., Warren, 1969; Benson and Akasofu, 1984). Using the RPI measurements, instantaneous locations of magnetospheric boundaries (magnetopause and plasmapause) and density profiles along a given radio echo ray path can be obtained by inverting the plasmagram trace.

The RPI on IMAGE will also be able to deduce magnetospheric properties at extremely large distances. A number of studies based on the Alouette/ISIS data have shown that signal enhancements of 20–40 dB (relative to vertical propagation) can be obtained from echoes resulting from waves guided along N_e field-aligned irregularities (Lockwood, 1973, and references therein). Such ducted echoes have been used to demonstrate the extended field-aligned nature of equatorial ionospheric bubbles and to determine N_e profiles within them (Dyson and Benson, 1978). Calvert (1981) has shown that a sounder capable of generating 5 μW within a magnetospheric duct would detect long-range magnetospheric echoes suitable for remote N_e measurements near the cusp and auroral zone and the detection of dayside compressions and nighttime expansions of the geomagnetic field.

RPI will also make precise local measurements of N_e and the electron temperature T_e by making use of sounder-stimulated plasma resonances and quasi-thermal noise measurements. These techniques will be described in more detail in the next two subsections.

4. *In situ* Measurements

The RPI is also a relaxation sounder, a low-power device that can make reliable *in situ* measurements by detecting short-range ($\sim<1$ km) electrostatic wave echoes (e.g., see Benson, 1977; Etcheto et al., 1981) at the various resonant frequencies of a plasma. It is expected that RPI will excite plasma resonances over its entire 3 kHz–3 MHz range corresponding to N_e values from 10^{-1} to 10^5 cm^{-3}.

In addition to the wealth of information on plasma resonances provided by high-power topside-sounder satellites (see the review by Benson, 1977), plasma resonances have been stimulated by relatively low-power devices. For example, rocket-borne ionospheric relaxation-sounders using short antennas (4 m tip-to-tip) and low power (2 W) detected short-duration (a few ms) resonances (Higel and de Feraudy, 1977). Satellite-borne magnetospheric relaxation-sounders applying

100 V to much longer antennas (40 m on GEOS 1 and 73.5 m on ISEE 1) detected extremely long-duration (100 ms) resonances (Etcheto et al., 1981). The longest duration nf_g resonances were observed at frequencies near f_p.

The RPI relaxation-sounder operations will permit determination of the local N_e and magnitude of **B** at the spacecraft. These local measurements will be used to improve the inversion of the sounder-reflection traces into N_e profiles. The local N_e and **B** will be determined mainly from the measured frequencies of the relaxation-sounder-stimulated plasma resonances at f_p, f_g, and nf_g (where $n = 2, 3, \ldots$). Other resonances, which can also be used to determine these parameters, are stimulated at frequencies between nf_g.

In this mode of operation, RPI should also be able to investigate wave-particle interactions and aid in the identification of wave modes of natural magnetospheric emissions. Relaxation-sounder stimulated resonances are observed both above and below f_p and have been related to natural emissions in the terrestrial magnetosphere (Oya, 1972; Christiansen et al., 1978; Benson and Osherovich, 1992). Plasma resonances have also been excited by the *Ulysses* relaxation sounder in the rapidly co-rotating plasma torus of Jupiter. Two different interpretations have been put forward to explain the observations (Osherovich et al., 1993a; Le Sager et al., 1998). RPI relaxation-sounder operations may provide observations that could help to resolve some of the questions raised by these investigations.

The RPI will also operate passively in order to receive natural magnetospheric emissions. The passive operations will eliminate possible confusion about the reception of echoes from active RPI transmissions. This mode of operation, coupled with active sounding, was found to be extremely valuable for the identification of natural ionospheric emissions using ionospheric topside-sounder data (see, e.g., Benson and Calvert, 1979; Benson, 1993).

4.1. *In situ* PLASMA MEASUREMENTS FROM QUASI-THERMAL NOISE SPECTROSCOPY

In a plasma, the particle thermal motion produces electrostatic fluctuations, which are completely determined by the velocity distributions. The resulting quasi-thermal noise spectrum around f_p can be measured with a sensitive receiver at the terminals of an electric antenna. The noise spectrum can also be used to measure N_e, T_e, and suprathermal electron parameters (Meyer-Vernet and Perche, 1989) and the plasma bulk speed (Issautier et al., 1999).

When f_g is sufficiently smaller than f_p, the electron thermal motions excite Langmuir waves and the quasi-equilibrium spectrum is cut off at f_p with a peak just above it. In addition, the electrons passing closer than a Debye length to the antenna induce voltage pulses on it, producing a plateau in the wave spectrum below f_p and a decreasing signal level above f_p. These parts of the spectrum are mainly determined by the bulk (core) electrons, which in turn mainly determine the Debye length. In contrast, since the Langmuir wave phase velocity becomes

very large near f_p, the fine shape of the peak is determined by the supra-thermal electrons.

This analysis technique, for the determination of N_e and T_e, has been used in a number of space environments and serves as a reference for other techniques (see the review by Meyer-Vernet et al., 1998. It has been used recently in the Earth's plasmasphere on Wind (Moncuquet et al., 1995) and on AMPTE (Lund et al., 1995), even though the instrumentation on these spacecraft had not been designed for this kind of study. Because the technique relies on a wave measurement, as in the case of the stimulated plasma resonances discussed above, it senses a large plasma volume and is relatively immune to the spacecraft potential and photoelectron perturbations which generally pollute particle analyzers and Langmuir probes. In addition, the measurement of the local density is simple and independent of gain calibrations, since one has only to locate the frequency of the peak amplitude. The main limitations of the technique are the Debye length and additional sources of noise. When the Debye length increases and approaches the antenna length, the line broadens and f_p and T_e become difficult to measure accurately; hence the antenna length should be much greater than the local Debye length. In addition, for measurements of the thermal T_e, the plasma thermal noise level on both sides of the peak and especially the plateau, must be larger than other sources of noise and the receiver must be well calibrated.

When f_g is not small compared to f_p, banded emissions are observed. These emissions have been interpreted as Bernstein-mode waves excited by electron thermal motion by Meyer-Vernet et al. (1993) to determine the absolute value of **B** and by Moncuquet et al. (1997) to determine f_p. An alternative interpretation of the banded emissions observed below f_p, which has also been used to determine f_p and the absolute value of **B**, has been presented by Benson et al. (1998a).

The N_e and T_e measurements in the plasmasphere and plasmapause should be of special interest. Few plasmaspheric T_e measurements have been performed making the comparison with theoretical models difficult. In particular, there is no consensus on the origin of the temperature increase observed in the plasmasphere with increasing L and of its anti-correlation with the plasma density. Some heating processes may be at work and/or the electron distribution is not at equilibrium. Under these conditions the ambipolar electric field may produce a temperature increase anti-correlated with the density (Scudder, 1992; Pierrard and Lemaire, 1996), as has been shown to be the case in magnetic clouds (Osherovich et al., 1993b) and in Jupiter's inner magnetosphere (Meyer-Vernet et al., 1995). The experimental setup is especially adapted to this study since it should measure N_e and T_e over a range covering several decades. In addition, the coupling of the thermal plasma with the ionosphere inside the plasmapause and with the remote magnetosphere and magnetosheath in the magnetospheric cavity region poses difficult problems that are still unsolved. The RPI quasi-thermal noise measurements will enable the variations in these coupling processes to be investigated under different magnetic, solar activity, and local time conditions. In the mag-

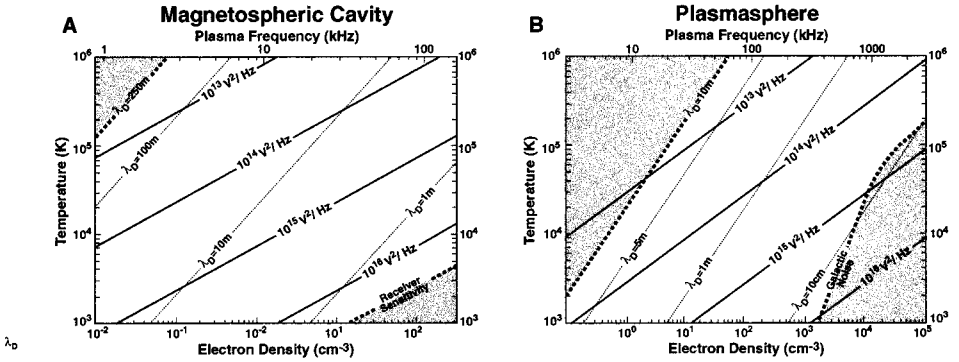

Figure 4. Domains in the density/temperature plane where both the electron density and temperature can be measured with the technique of quasi-thermal noise spectroscopy. (A) is for the X and Y-axis antenna and (B) is for the Z-axis antenna. In the gray regions, the temperature cannot be measured accurately because either the Debye length is too large (left side) or the plateau spectral density below the peak is smaller than the receiver noise or the galactic noise. The dotted lines are isocontours of the Debye length; the continuous lines are isocontours of the spectral density of the plateau below the plasma frequency.

netospheric cavity and the polar cusp, however, the electron velocity distribution may be very anisotropic which may reduce the accuracy of the quasi-thermal noise measurements.

The expected dynamic range of the quasi-thermal noise technique in the density-temperature domain is shown in Figure 4. Panel A is for the X- and Y-axis antenna, and panel B is for the Z-axis antenna. The domains shown in gray are those where the temperature cannot be measured accurately because of Debye length limitation (on the low-density large-temperature side), or because the plateau of the spectrum is lower than the receiver sensitivity or the galactic noise (on the high-density small-temperature side). The plasma density can be measured in a larger range of parameters, because it requires only that the top of the peak emerge from the other noise contributions. We have also drawn isocontours of the spectral density for each decade, showing the limit below which no other signal, and in particular the echoes, can be measured. Two additional limitations have not been drawn on the figure because they depend on the operation mode and magnetospheric conditions. The first limitation is due to the frequency limits of the receiver (lower limit of 3 kHz in most cases, corresponding to $N_e = 0.1$ cm^{-3}). The second one is the occurrence of transitory natural radio emissions; this latter limit is less stringent because such emissions do not pollute the plateau in the spectrum below f_p, so that they do not affect the measurement of N_e but only reduce the accuracy of T_e measurements.

5. Expected Science Results from RPI Observations

RPI will observe several magnetospheric plasma regions and boundaries simultaneously. Using the RPI, measurements of echoes of omni-directional transmissions of radio waves at various frequencies will yield the density profiles between the spacecraft and different remote plasma regimes along different directions. These echoes can be distinguished by their time delay-frequency characteristics, Doppler shifts and angles-of-arrival (Reinisch et al, 1998, 1999), as concurrent conditions of the inner and outer magnetosphere can thus be observed. Since the echo delay times ($<$seconds) are typically shorter than the plasma dynamical time scales, density profiles obtained from RPI measurements in different directions can be used to obtain an 'instantaneous view' of magnetospheric boundary region structures. We outline in the following subsections some expected science results pertaining to the different magnetospheric regions that can be probed by the RPI on IMAGE.

5.1. Magnetopause and boundary layer

The 8-R_E apogee of the IMAGE spacecraft over the polar region is a favorable location from which to observe the magnetopause and other magnetospheric boundary regions such as the plasmapause, cusp and plasma mantle, as illustrated in the ray tracing simulations of Figure 2. RPI echoes will yield information on the position and internal structures (e.g., density and thickness) of the magnetopause and boundary layer (see Figure 3). RPI has the ability to make repetitive high time-resolution magnetopause echo measurements from a remote location. A plasma density measurement will be derived from each echo (see Figure 3). In addition, RPI has the ability to make direction of arrival and Doppler measurements, thereby being able to separate time and spatial variations of the magnetopause region that are already known to exist under various solar wind conditions.

Unlike most *in situ* observations of the magnetopause by single- or dual-spacecraft missions that can only provide information on small-scale structures, the RPI can provide observations of large-scale variations in the magnetopause, its wave structure, and its motion. Figure 5 shows a schematic illustrating the reflection of multiple echoes from a large-scale surface wave in the magnetopause-boundary layer region. In addition, previous observations of the thickness of the magnetopause vary from less than 100 km to more than 1000 km, while that of the boundary layer can be an Earth radius or more. The substantial uncertainties in these thicknesses are largely caused by the temporal and spatial aliasing of *in situ* observations due to the finite resolutions of the instruments and dynamical nature of the magnetospheric boundary plasmas.

The ratio of the magnetopause thickness to boundary layer thickness can be used to test competing models for the generation and maintenance of the structure of the magnetopause and boundary layer, such as shear driven MHD instabilities, drift-wave instabilities, cross-field streaming instabilities, and reconnection.

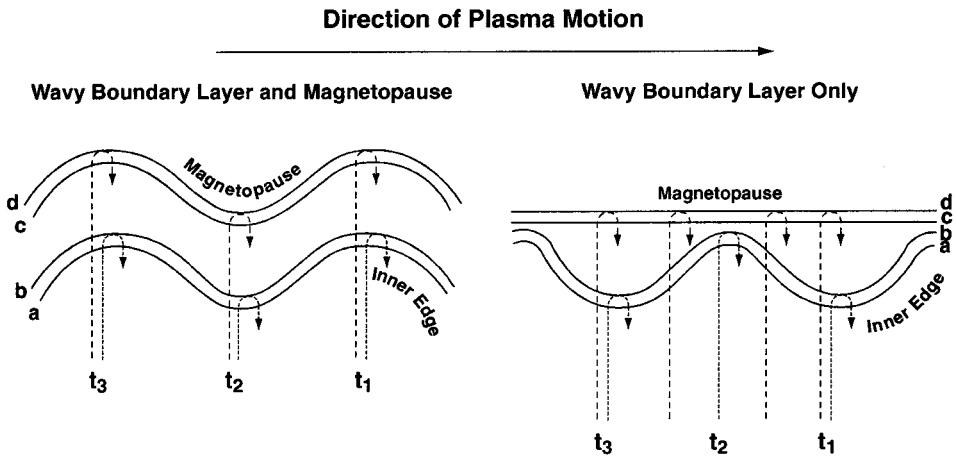

Figure 5. Schematic of the wave structure at the magnetopause.

Unlike *in situ* measurements in which passages through the magnetopause and boundary layer regions are limited by specific orbital positions, echoes from these regions will be easily found in the RPI data. Near apogee, RPI will be able to obtain several hundred density profiles of the magnetopause region from more than one direction simultaneously. These RPI measurements would correspond in terms of information content to the entire lifetime of magnetopause measurements on an *in situ* mission. Statistical studies will determine the magnetopause to boundary layer thickness ratio over varying solar wind conditions.

5.2. POLAR CUSP

The cusp is a dynamic region where much of the solar wind-magnetosphere interaction occurs (Potemra, 1992; Yamauchi et al., 1995). Yet its structure and dynamics have not been clearly delineated and understood, particularly with regard to how these characteristics change with altitude, longitude and latitude (Fung et al., 1997). The RPI will provide unprecedented three-dimensional observations of the cusp region and will perform, for the first time, detailed remote sensing of time-dependent magnetosheath particle injection into the cusp.

Heretofore, cusp observations have been limited to *in situ* measurements, which are at the mercy of the observing satellite orbits, cusp motions induced by changing interplanetary magnetic field (IMF) and solar wind pressures, and the apparently erratic injection processes. With the RPI's capability of monitoring the cusp global density structure on a few minute time scale, we can resolve the question of whether cusp plasma injection is quasi-steady or impulsive (Crooker and Burke, 1991; Newell, 1995). If the injection is quasi-steady, the cusp density structure should be reasonably stable, with a sharp density increase on the equatorward side and a gradual decay on the poleward side (Xue et al., 1997). The RPI range and

Doppler measurements will be used to determine the changes in the cusp position in response to variable solar wind conditions.

An injection pulse during southward IMF should create a characteristic sudden equatorward motion of the cusp low latitude edge and a sudden increase in cusp ion fluxes at the equatorward edge caused by the addition of newly injected plasma. After each new injection, the cusp ions will be convectively dispersed poleward and their densities will gradually decay. The dynamical changes in the associated electron plasma structure (Escoubet et al., 1995) can be investigated by using the RPI range and Doppler measurements.

Since every new injection will generally give rise to the highest cusp density (e.g., Escoubet et al., 1992), the cusp peak density will likely occur on the 'fresh' equatorward injection site. Thus the best viewing location is probably on the poleward side of the cusp, from which each preceding layer can be separately sounded. During northward IMF, reconnection can occur poleward of the cusp (Kessel et al., 1996), a situation that can be investigated by the RPI when IMAGE is located on the cusp's equatorward side. In addition, by sounding in both the ordinary and extraordinary modes, it should be possible to elucidate the relationship between the magnetic and plasma characteristics of the cusp region.

5.3. PLASMAPAUSE AND PLASMASPHERE

This section will discuss the anticipated results from RPI measurements of the plasmasphere. The RPI can observe plasmaspheric structure by performing remote radio sounding from outside the plasmasphere and local relaxation sounding and thermal noise measurements from within the plasmasphere (see Section 4). Of particular interest will be plasmasphere and plasmapause structure and dynamics.

5.3.1. *Plasmasphere Erosion and Recovery*

Experimental work to date has yielded much information about the various states of the plasmasphere system but has left us with only limited evidence and understanding of the physical processes involved in plasmasphere erosion/recovery cycles (e.g., Carpenter and Lemaire, 1997; Lemaire and Gringauz, 1998). For instance, we do not know how and where a plasmapause boundary is formed at a new location during a period of enhanced disturbance activity. We want to know what kinds of erosive effects occur at or near the nightside interface between the cool plasmasphere and the inner edge of the plasma sheet. Are subauroral ion drifts (SAIDs) (e.g., Anderson et al., 1991; 1993) important in plasmasphere erosion, as has been suggested (e.g., Carpenter et al., 1993; Ober et al., 1997)?

We need tools capable of investigating on a global scale and at various stages of erosion and recovery the interplay between solar wind-induced magnetospheric convection and the Earth's rotation. It is known that in the aftermath of geomagnetic disturbances, complex density structures can develop in the region of plasmapause density gradients and in the outer plasmasphere (e.g., Park and Carpenter,

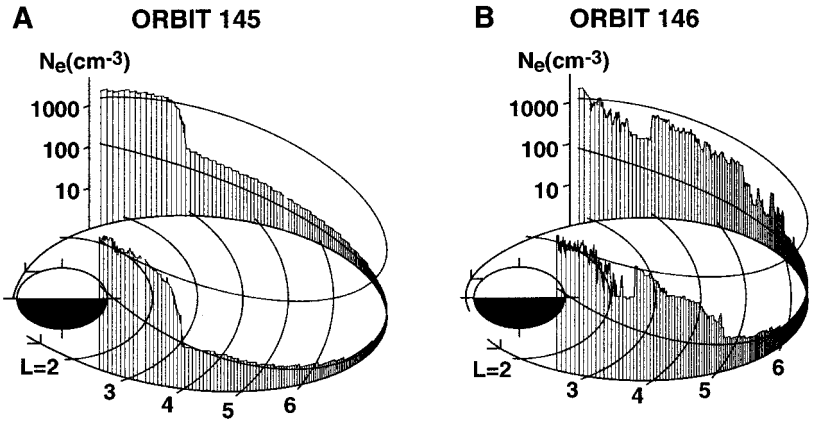

Figure 6. Plots showing electron density along two successive near-equatorial orbits of CRRES on September 23–24, 1990. Log electron density is plotted vertically against L value and MLT (adapted from Carpenter, et al. (1999).

1970; Oya and Ono, 1987; Koons, 1989; Horwitz et al., 1990; Carpenter et al., 1993; LeDocq and Gurnett, 1994; Moldwin et al., 1995). Under what global and local conditions does such structure develop? Do instabilities play an important role in the plasmasphere erosion process, as has been suggested (e.g., Lemaire, 1975; Lemaire and Gringauz, 1998)?

In the aftermath of a period of enhanced convection, plasma density in the outer part of the eroded plasmasphere is usually found to be reduced, in some locations by a factor of up to three (e.g., Park and Carpenter, 1970; Carpenter et al., 1993). Does this additional plasma loss involve flow along **B** into the ionosphere, or a convective loss to the magnetopause? As the plasmasphere and plasmatrough regions recover from density depletion, what is the interplay between coupling fluxes from the ionosphere and magnetospheric convection?

The RPI and the EUV instruments on IMAGE will be operating in complementary fashion as they are used to address these challenging questions (for information about EUV, see Sandel et al., this issue). Some of the complexities that they will encounter are illustrated in Figure 6, which shows electron density along two successive near-equatorial CRRES satellite orbits in the post-midnight/morning sector. The orbits are displayed in coordinates of L value versus magnetic local time, while the density values, inferred from sweep frequency receiver (SFR) records (e.g., Gurnett and Shaw, 1973), are plotted vertically on a log scale along the orbital tracks (Carpenter et al., 1999). The upper and lower curves that follow the density 'wall' are from an empirical model of the quiet plasmasphere and of the nighttime plasmatrough region, respectively (Carpenter and Anderson, 1992). The orbits occurred $\sim$10 hours apart during a period of quieting following an earlier episode of plasmasphere erosion. During orbit 145 the form of the density distribution was very simple, with a well-defined plasmapause and well behaved profiles within the

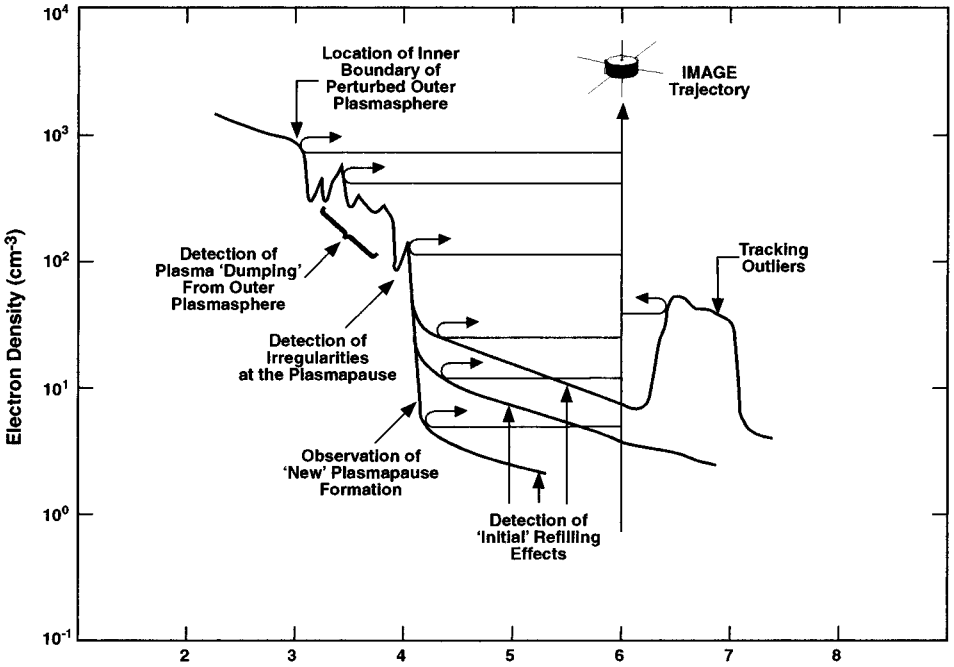

Figure 7. Schematic drawing of various aspects of plasmasphere structure and dynamics that may be investigated by radio sounding.

plasmasphere and in the plasmatrough (magnetospheric cavity) region. However, during orbit 146, dense plasma extended farther in L value and in general the profile was much more structured on scales ranging from ~100 to 10 000 km. Density troughs appeared both inbound and outbound in the $L = 3–4$ range. This is a nice example of the rapidity with which the density distribution in a given local time sector can change.

Many of the differences, shown in Figure 6, between orbits 145 and 146 may be attributed to transport into the morning sector of plasma structure imposed in an earlier MLT sector, most likely near dusk. In a comparable situation on IMAGE the idea would be to use EUV observations from near apogee of the He^+ component of the plasmasphere to obtain global scale images of the plasmasphere shape and of its major temporal changes over a several hour period. Then RPI, during a 3- to 4-hour period inbound or outbound, would sound the plasmasphere over a longitude range near the current IMAGE orbital plane, mapping changes in the profile that occur as the Earth's corotation electric field carries new structure into the range of the sounder or as changes occur as a result of local cross-L plasma motions or instabilities. By combining the results from EUV and RPI in cases such as this, it should be possible to gain important new insights into the various transport processes that affect the plasmasphere.

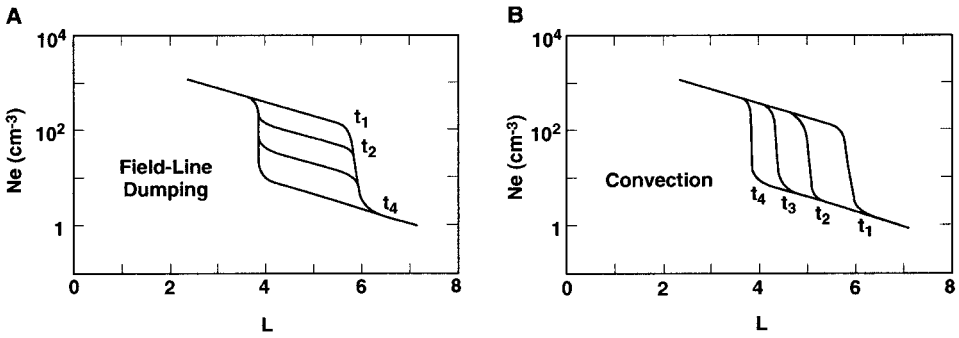

Figure 8. Sketches of changes with time in plasmapause L value associated with plasma loss to the ionosphere (A) and motions transverse to **B** (B).

Figure 7 shows in idealized fashion a number of RPI measurement objectives pertinent to the science questions raised above. The topics pursued would vary in detail depending upon the magnetic local time at the IMAGE position and the orientation of the orbit with respect to the plasmasphere. For example, certain regions on the nightside, and possibly dusk side, may afford better insights into new plasmapause formation and the early stages of density refilling. Irregularities at or near the plasmasphere surface may appear at essentially any local time. Their interpretation and that of many phenomena studied remotely will be enhanced by the ability of RPI to make local measurements along the IMAGE orbit and to do so as the spacecraft penetrates or closely approaches the plasmasphere boundary (Fung et al., 2000).

In addition to information on the location of the plasmapause, RPI will acquire information on the density profiles on either side of the boundary. The value of these measurements is illustrated in the simplified sketches of Figure 8, which show two ways in which the boundary can be displaced inward, by motion transverse to **B** (panel B) and by interchange with the ionosphere along **B** (panel A). The manner in which the density profile appears to RPI at successive time intervals should provide important information on these possibly competing effects.

The sketch of Figure 9 shows an IMAGE orbit early in the mission lifetime. Apogee is in the afternoon sector. Major features indicated are the plasmasphere, dense outliers, and a 'plasmaspheric cavity' (the latter two are discussed below). The satellite will approach or penetrate the plasmasphere twice during an orbit, at a relatively low altitude near perigee on one side of the Earth and at an altitude of several Earth radii on the other. On the upleg, for $\sim$3 to 4 hr along section C and part of D, it should be possible to detect the plasmapause over a range of longitudes and relatively high latitudes. At times during this period, relatively strong echoes may be received due to focusing associated with the concave curvature of the plasmasphere in the azimuthal direction. However, it may not be possible to measure the density profile to points deep within the plasmasphere because of the generally radial orientation of the refractive index gradients in that region.

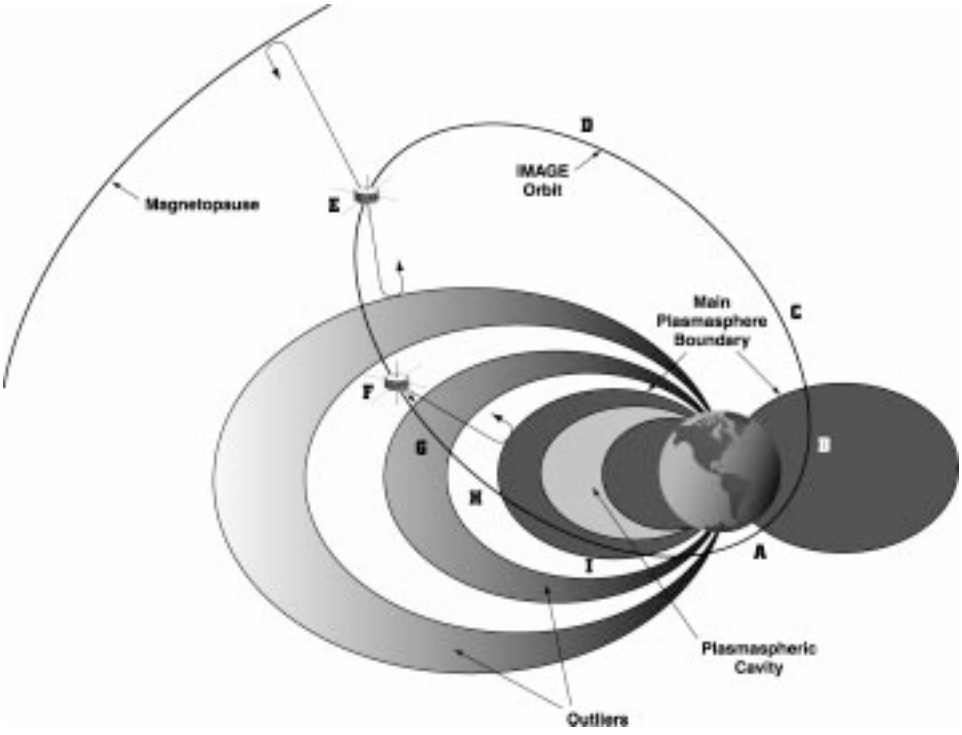

Figure 9. Diagram of an IMAGE orbit early in the mission lifetime, showing afternoon-sector conditions on the downleg (sections E through I). Dense plasma outliers and a plasmaspheric cavity are indicated.

Sections E, F, G, and H of the downleg (∼4 hr) of IMAGE's orbit, in Figure 9, will be used for detecting the plasmapause and its dynamics. In particular, the period when the satellite is in the plasmatrough and at a magnetic latitude less than ∼30° (F, G, and H) will be favorable for obtaining echoes from deep within the plasmasphere.

5.3.2. *The Plasmasphere and Dense Outliers*

It is well known from a combination of whistler and satellite data that dense plasmas in the afternoon and dusk sectors are entrained generally sunward and outward during periods of enhanced convection activity (e.g., Carpenter, 1970; Chappell, 1974; Carpenter and Seely, 1976; Lennartsson and Reasoner, 1978, Moldwin et al., 1994), observations from synchronous orbit being particularly extensive in this regard (e.g., Higel and Wu, 1984; Moldwin et al., 1994; Elphic et al., 1997; Weiss et al., 1997). An example of the complex outlying structure that can be observed along a near-radial satellite trajectory is shown on the ISEE density profile of Figure 10. The position of the satellite in geocentric distance vs. MLT is indicated on the inset. The profile shows irregular structure at the plasmapause, an only slightly structured outlier near $L = 6$, and then a patchy, irregular region of dense plasma

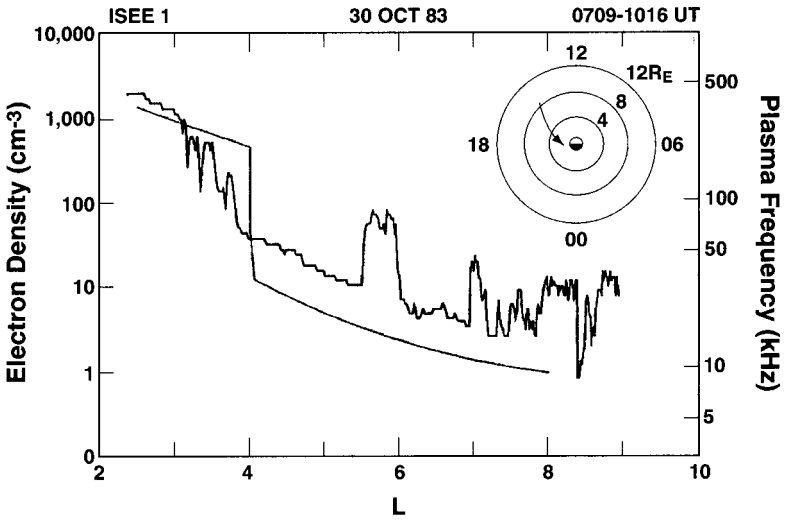

Figure 10. Near-equatorial electron density profile obtained by ISEE along the orbit shown in the inset. A corresponding plasma frequency scale is shown at the right (from Carpenter et al. (1993)).

beyond $L = 7$. Plasma frequencies corresponding to the density scale on the left are shown at the right.

In spite of the regularity with which outliers have been encountered, particularly at synchronous orbit, little is known about their form and large scale distribution. Limited evidence (e.g., Taylor et al., 1970; Ho and Carpenter, 1976; Carpenter et al., 1992) suggests that some may be tail-like, connected to the main body of the plasmasphere, as in the Rice Convection Modeling work (Spiro et al., 1981) while others may be effectively detached from that body, as inferred in the work by Chappell et al. (1971) and by Chappell (1974). The evidence also suggests that the evacuation process, involving flow of dense plasmas into the magnetopause boundary layers, can be inefficient, and that islands or longitudinally extensive belts of dense plasma several Earth radii in radial extent may exist in the outer afternoon-dusk magnetosphere for extended periods following the onset of a plasmasphere erosion episode (Carpenter et al., 1993). Through combined use of the RPI and EUV instruments on IMAGE, it should be possible to map the shapes of outliers and to observe their development and motions. From such data, important new knowledge may be gained about the amount of plasma removed from the outer plasmasphere during periods of enhanced convection activity, about the process of removal, and about the transport and fate of the removed plasmas. Overall, the results should provide unique information on the relationship of outlier activity to the behavior of the magnetopause and the plasmasphere.

The sketch of Figure 9 shows how RPI may be used to study the outlier phenomenon in the early lifetime of IMAGE. From directional and Doppler information on echoes received near E, the spatial relationship of the outermost detected outlier to the magnetopause may be determined. In some cases that outlier may be essentially

adjacent to the magnetopause. Along orbital segments E, F, G, and H, echoes from both outliers and the main plasmasphere may be used in combination with local density data to determine whether certain outliers are effectively detached from the main plasmasphere and thus limited in longitudinal extent or are connected to the plasmasphere by spiraling tail-like forms. In these observations information on echo arrival bearing will be of particular importance.

When an outlier is probed from a position between it and the magnetopause, its internal density profile can be investigated (the density should generally increase with decreasing L value). When probed from inside, that is from the direction of the main plasmasphere, longitudinally extended outliers may provide excellent echoes because of a concave inward overall shape (and the real possibility of having surface irregularities with scale larger than a Fresnel zone, see e.g., Fung et al., this issue).

5.3.3. *Plasmasphere Density Cavities*

Deep density troughs, in which electron density was a factor of from ~2 to 10 below nearby plasmasphere levels, were found during ~13% of 1764 plasmasphere crossings documented in sweep frequency receiver (SFR) data acquired in 1990-1991 on the CRRES satellite (Carpenter et al., 1999). Reported previously by Horwitz et al. (1990) from DE-1 data, these 'inner troughs' appeared in the aftermath of plasmasphere erosion episodes. Interpreted as the near-equatorial manifestations of plasmaspheric cavities, they were found at all local times, but were most common in the ~18–24 MLT sector. While their plasmapause-like inner boundaries were mostly at $L < 3.5$, in ~30% of the cases they were at $L < 2.5$ under geomagnetic conditions that traditionally have been associated with plasmapause radii in the $L = 3$–3.5 range or beyond. For example, in Figure 6 the data for CRRES orbit 146 show trough effects in the $L = 3$–4 range both outbound and inbound. In contrast, Figure 11 provides an example of a well-defined trough in the pre-midnight sector in which the density depression extended from $L \sim 2.3$ to $L \sim 3.8$. On both orbits 146 and 1033 the dense regions beyond the troughs exhibited a variety of irregular features.

The trough outer walls were found to be exceptionally steep: in several cases there was a factor of 4 or more density change within less than 100 km along the near-equatorial CRRES orbit. The extent of the troughs in L ranged from $\Delta L \sim 0.5$ to ~2, and extents of more than 20° in longitude were inferred. In many cases, radio noise appeared to be trapped within the cavity. It typically extended in frequency well above the usual ~50 kHz upper limit of trapped continuum radiation detected beyond the plasmasphere.

The observed troughs are believed to be translated vestiges of plasma configurations established during preceding periods of plasmasphere erosion (e.g., Carpenter et al., 1999). They are clearly related to global plasmaspheric dynamics, and their investigation becomes important for gaining an overall understanding of the plasmasphere. Outstanding questions are: (1) Where and when do troughs develop

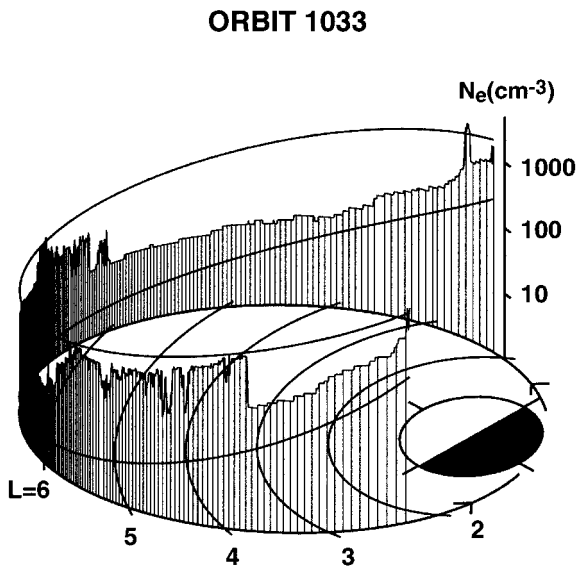

Figure 11. Plot in format similar to that of Figure 6 showing an example of an inner trough in the premidight sector observed from the CRRES satellite on September 27, 1991. The viewpoint is along the 21 MLT meridian (adapted from Carpenter et al. (1999)).

within the plasmasphere? (2) What physical mechanisms govern the development of inner troughs and the formation of their density profiles? (3) What can we learn from the troughs about the penetration of magnetospheric convection to subauroral latitudes near L=2 under geophysical conditions normally associated with penetration limits at higher L? and (4) What is the nature of the radio noise found within some inner troughs?

Figure 9 provides a basis for seeing how IMAGE can address these important questions. From points near apogee (positions D and E), the full complement of IMAGE instruments may observe the geophysical conditions in which a plasmasphere erosion episode occurs. In some cases, erosion to the vicinity of $L = 2$ should be observed, at least within some limited longitude range. Then RPI, when inbound at F, G, or H during various stages of the erosion event and recovery therefrom, will sound the plasmapause as it probes the interior of the plasmasphere for evidence of a cavity. Such a feature should produce distinctive plasmagram signatures as the sounding frequency approaches the peak plasma frequency in the region outside the trough. Carpenter et al. (1999) has found strong natural wave emissions trapped in the plasmaspheric cavity. If a cavity is penetrated by IMAGE on either an inbound or outbound leg, its presence and structure may best be revealed in relaxation sounding data, in ambient thermal noise receptions within the troughs, and in active or passive operations at whistler-mode frequencies.

Overall, the observations from IMAGE should open a new chapter in our understanding of the subauroral action of convection electric fields during and following

episodes of plasmasphere erosion. From measurements on a single orbit, we should learn much about the variations in trough width and the density structure of a trough inner wall as the plasmasphere region involved rotates or partially rotates with the Earth. From measurements on successive orbits, we should learn much about how cavities evolve. IMAGE will help answer questions about cavity morphology, such as the longitudinal extent of a cavity, the degree to which the outer belt of plasma is detached from the main plasmasphere, and the as yet unknown geophysical circumstances under which the inner edge of the cavity can be located at $L < 2.5$.

5.4. MAGNETOSPHERIC WAVE EMISSIONS

When operating in the passive mode, the RPI will be able to measure natural wave emissions, such as solar radio bursts, auroral kilometric and continuum and Z mode radiation, as well as the whole host of magnetospheric plasma waves intercepting the IMAGE orbit.

Banded magnetospheric emissions, for example, have been observed in every planetary magnetosphere visited by spacecraft (Kurth, 1992 and reference therein). Although they are commonly attributed to unstable electrostatic Bernstein-mode waves, there remain several fundamental difficulties with this interpretation. Firstly, Bernstein modes are 'electrostatic' but the banded magnetospheric waves have been observed to exhibit a small magnetic-field component (Matsumoto and Usui, 1997). Secondly, one of the observed frequency bands has been inferred to correspond to the upper-hybrid frequency (e.g., see Birmingham et al., 1981) although there has not been a reliable independent way of determining this frequency. Thirdly, multiple emissions are often observed between adjacent harmonics of the local f_g (e.g., see Koons and Fennell, 1984), an observation that can only be explained by invoking very special plasma conditions.

Alternate interpretations of banded emissions have been proposed based on interpretations of ionospheric topside sounder observations. It has been suggested that ionospheric topside sounder stimulated wave-particle interactions can lead to wave emissions with spectra similar to the magnetospheric banded emissions (Benson and Osherovich, 1992, and references therein). The wave emission process strongly depends on specific values of the electron plasma-to-cyclotron frequency ratio that can be satisfied in vastly different plasmas such as the Earth's ionosphere and magnetosphere and Jupiter's Io plasma torus. Topside-sounder observations indicate that one class of these emissions actually occurs at frequencies below the electron plasma frequency when this ratio is between 2 and 8.

With the RPI, we expect to determine responsible physical processes and the relationship between many magnetospheric wave emissions, such as the escaping continuum, trapped continuum, and banded or $(n + 1/2)\ f_g$ emissions. Since these emissions are not limited to the terrestrial environment, understanding the processes operating in the terrestrial ionosphere/magnetosphere system will likely be relevant to understanding the basic process at work in other magnetized space

plasmas. In addition, the wave mode of the banded emissions will be identified using RPI relaxation sounding and thermal noise measurements. This identification will be based on stimulating echoing electrostatic waves (often called local plasma resonances) and electromagnetic wave cutoffs in order to accurately determine the ambient electron density and magnetic field strength based on the Alouette/ISIS experience, where the plasma parameters were determined to within a few percent.

The ISIS topside sounders commonly observe both natural and sounder-generated Z-mode waves (e.g., see James, 1979; Benson, 1985, 1993, 1997, and references therein). In the general case, for propagation at an angle with respect to the ambient magnetic filed, the Z mode wave can propagate between f_p (the L mode cut-off) and the upper hybrid frequency. The lower frequency cutoff for the Z mode is the lower hybrid frequency, which is much less than the f_p. Based on the experience gained from the ISIS topside sounders, it is certain that Z mode waves will be generated along with the other wave modes. When the spacecraft is in the polar cap at relatively low altitudes, the Z mode transmissions will be of particular interest for two reasons. First, the frequency may be high enough to enable sufficient power to be radiated in this mode so as to provide additional information about the structure of ionospheric or auroral plasma cavities. Second, efficient ducted propagation nearly along the magnetic field direction could be directed nearly vertical downward. Examples of the dispersion for Z mode waves, and of ray tracing of Z mode waves in the topside ionosphere out to 2 R_{E} are given in Horne (1995). It may be possible to test out the two mechanisms suggested by Horne (1995) whereby energy in Z mode waves could be observed on the ground, one via mode conversion, the other by direct propagation under conditions of very low plasma density.

6. Conclusions

The RPI instrument on the IMAGE mission is a swept frequency adaptive sounder, with on-board signal processing which transmits and receives coded electromagnetic pulses over the frequency range from 3 kHz to 3 MHz. The primary mode of operation for RPI is to generate radio pulses that propagate as free space waves through the magnetosphere and are reflected upon encountering their plasma cutoff frequencies. The RPI will measure the amplitudes, Doppler shift, and direction of arrival as a function of frequency and echo delay. The echo arrival angles will be calculated from the amplitudes and phases of the signals from three orthogonal receiving dipole antennas. In addition, at locations where the frequency of the sounder is below the plasma frequency, RPI will stimulate the local plasma providing detailed *in situ* measurements acting as a relaxation sounder.

Ray tracing calculations have been used to determine the feasibility and limitations of the RPI and to simulate the frequency time structure of the returning RPI echoes which will greatly aid in the analysis of the actual data. At times when

RPI is situated in the density cavity of the magnetosphere, the ray tracing calculations illustrate how RPI will be able to simultaneously determine the location and dynamics of remote boundaries such as the plasmapause and magnetopause. In addition, the RPI would be able to provide N_e profiles in different directions on time scales of a few minutes or less. At specific sounder frequencies, characteristic of remote plasma regions where large-scale oscillations are occurring within the range of RPI, images of the magnetospheric structures should be possible. In summary, the RPI should be able to provide unprecedented global magnetospheric observations.

Acknowledgements

The work at Rice University was supported by NASA under subcontract to Southwest Research Institute, and at Raytheon ITSS under NASA contract NASW-97002.

References

Aikyo, K. and Ondoh, T.: 1971, 'Propagation of Nonducted VLF Waves in the Vicinity of the Plasmapause', *J. Radio Res. Labs.* **18**, 153.

Anderson, P. C., Heelis, R. A. and Hanson, W. B.: 1991, 'The Ionospheric Signatures of Rapid Subauroral Ion Drifts', *J. Geophys. Res.* **96**, 5785.

Anderson, P. C., Hanson, W. B., Heelis, R. A., Craven, J. D., Baker, D. N. and Frank, L. A.: 1993, 'A Proposed Production Model of Rapid Subauroral Ion Drifts and Their Relationship to Substorm Evolution', *J. Geophys. Res.* **98**, 6069.

Angerami, J. J. and Thomas, J. O.: 1964, 'The Distribution of Ions and Electrons in the Earth's Exosphere', *J. Geophys. Res.* **69**, 4537.

Benson, R. F.: 1977, 'Stimulated Plasma Waves in the Ionosphere', *Radio Sci.* **12**, 861–878.

Benson, R. F.: 1985, 'Field-Aligned Electron Density Irregularities Near 500 km – Equator to Polar Cap Topside Sounder *Z* Mode Observations', *Radio Sci.* **20**, 477.

Benson, R. F.: 1993, 'Elusive Upper Hybrid Waves in the Auroral Topside Ionosphere', in R. L. Lysak (ed.), *Auroral Plasma Dynamics,* Geophysical Monograph 80, American Geophysical Union, Washington, D.C., pp. 267–274.

Benson, R. F.: 1997, 'Evidence for the Stimulation of Field-Aligned Electron Density Irregularities on a Short Time Scale by Ionospheric Topside Sounders', *J. Atm. and Solar-Terr. Phys.* **59**, 2281.

Benson, R. F. and Akasofu, S.-I.: 1984, 'Auroral Kilometric Radiation/Aurora Correlation', *Radio Sci.* **19**, 527.

Benson, R. F. and Calvert, W.: 1979, 'ISIS 1 Observations at the Source of Auroral Kilometric Radiation', *Geophys. Res. Lett.* **6**, 479.

Benson, R. F. and Osherovich, V. A.: 1992, 'High Order Stimulated Ionospheric Diffuse Plasma Resonances – Significance to Magnetospheric Emissions', *J. Geophys. Res.* **97**, 19,413.

Benson, R. F., Fainberg, J., Hess, R. A., Osherovich, V. A. and Stone, R. G.: 1997, 'An Explanation for the Absence of Sounder-Stimulated Gyroharmonic Resonances in the Io Plasma Torus by the *Ulysses* Relaxation Sounder', *Radio Sci.* **32**, 1127.

Benson, R. F., Osherovich, V. A., Fainberg, J., MacDowall, R. J. and Stone, R. G.: 1998a, 'Magnetospheric '$(n + 1/2)$' Emissions Observed Both Above and Below the Electron Plasma Frequency', *Suppl. Eos Trans. AGU* **79**, F690.

Benson, R. F., Green, J. L., Fung, S. F., Reinisch, B. W., Calvert, W., Haines, D. M., Bougeret, J.-L., Manning, R., Carpenter, D. L., Gallagher, D. L., Reiff,, P. H. and Taylor, W. W. L.: 1998b, 'Magnetospheric Radio Sounding in the 21st Century', *Radio Sci. Bull.* **28**, 9.

Birmingham, T. J., Alexander, J. K., Desch, M. D., Hubbard, R. F. and Pedersen, B. M.: 1981, 'Observations of Electron Gyroharmonic Waves and the Structure of the Io Torus', *J. Geophys. Res.* **86**, 8497.

Breit, G. and Tuve, M. A.: 1926, 'A Test for the Existence of the Conducting Layer', *Phys. Rev.* **28**, 554.

Calvert, W.: 1981, 'The Detectability of Ducted Echoes in the Magnetosphere', *J. Geophys. Res.* **86**, 1609.

Calvert, W., Benson, R. F., Carpenter, D. L., Fung, S. F., Gallagher, D. L., Green, J. L., Haines, D. M., Reiff,, P. H., Reinisch, B. W., Smith, M. F. and Taylor, W. W. L.: 1995, 'The Feasibility of Radio Sounding in the Magnetosphere', *Radio Sci.* **30**, 1577.

Carpenter, D. L.: 1970, 'Whistler Evidence of the Dynamic Behavior of the Duskside Bulge in the Plasmasphere', *J. Geophys. Res.* **75**, 3837.

Carpenter, D. L. and Anderson, R. R.: 1992, 'An ISEE/Whistler Model of Equatorial Electron Density in the Magnetosphere', *J. Geophys. Res.* **97**, 1097.

Carpenter, D. L. and Lemaire, J.: 1997, 'Erosion and Recovery of the Plasmasphere in the Plasmapause Region', *Space Sci. Rev.* **80**, 153.

Carpenter, D. L. and Seely, N. T.: 1976, 'Cross-L Plasma Drifts in the Outer Plasmasphere: Quiet Time Patterns and Some Substorm Effects', *J. Geophys. Res.* **81**, 2728.

Carpenter, D. L., Smith, A. J., Giles, B. L., Chappell, C. R. and Decreau, P. M. E.: 1992, 'A Case Study of Plasma Structure in the Dusk Sector Associated with Enhanced Magnetospheric Convection', *J. Geophys. Res.* **97**, 1157.

Carpenter, D. L., Giles, B. L., Chappell, C. R., Decreau, P. M. E., Anderson, R. R., Persoon, A.M., Smith, A. J., Corcuff, Y. and Canu, P.: 1993, 'Plasmasphere Dynamics in the Duskside Bulge Region: a New Look at an Old Topic', *J. Geophys. Res.* **98**, 19243.

Carpenter, D. L., Anderson, R. R., Calvert, W. and Moldwin, M. B.: 1999, 'CRRES Observations of Density Cavities within the Plasmasphere', *J. Geophys. Res.* (submitted).

Chappell, C. R., Harris, K. K. and Sharp, G. W.: 1971, 'The Dayside of the Plasmasphere', *J. Geophys. Res.* **76**, 7632.

Chappell, C. R.: 1974, 'Detached Plasma Regions in the Magnetosphere', *J. Geophys. Res.* **79**, 1861.

Christiansen, P., Gough, P., Martelli, G., Bloch, J.-J., Cornilleau, N., Etcheto, J., Gendrin, R., Jones, D., Beghin, C. and Decreau, P.: 1978, 'Geos I: Identification of Natural Magnetospheric Emissions', *Nature* **272**, 682.

Crooker, N. U. and Burke, W. J.: 1991, 'The Cusp/Cleft', *Rev. Geophys. Suppl.* U.S. National Report to IUGG, 1017–1027.

Dyson, P. L. and Benson, R. F.: 1978, 'Topside Sounder Observations of Equatorial Bubbles', *Geophys. Res. Lett.* **5**, 795.

Elphic, R. C., Weiss, L. A., Thomsen, M. F. and McComas, D. J.: 1997, 'Evolution of Plasmaspheric Ions at Geosynchronous Orbit During Times of High Geomagnetic Activity', *Geophys. Res. Lett.* **23**, 2189.

Escoubet, C. P., Smith, M. F., Fung, S. F., Anderson, P. C., Hoffman, R. A., Basinska, E. M. and Bosqued, J. M.: 1992, 'Staircase Ion Signature in the Polar Cusp: a Case Study', *Geophys. Res. Lett.* **19**, 1735.

Escoubet, C. P., Smith, M. F., Fung, S. F., Hoffman, R. A. and Bosqued, J. M.: 1995, 'Electron Structures in the Cusp/Cleft RRegion Observed by DE 2 Satellite', *J. Geophys. Res.* **100**, 1597.

Etcheto, J., de Feraudy H. and Trotignon, J. G.: 1981, 'Plasma Resonance Stimulation in Space Plasmas', *Adv. Space Res.* **1**, 183.

Fung, S. F. and Green, J. L.: 1996, 'Global Imaging and Radio Remote Sensing of the Magnetosphere, Radiation Belts: Models and Standards', *AGU Monograph* **97**, 285.

Fung, S. F., Benson, R. F., Carpenter, D. L., Reinisch, B. W. and Gallagher, D. L.: 2000, 'Investigations of Irregularities in Remote Plasma Regions by Radio Sounding: Applications of the Radio Plasma Imager on IMAGE', *Space Sci. Rev.* **91**, 391–419 (this issue).

Fung, S. F., Eastman, T. E., Boardsen, S. A. and Chen, S.-H.: 1997, 'High-Altitude Cusp Positions Sampled by the Hawkeye Satellite', in *Proc. First Alfvén Conference on Low-Latitude Magnetospheric Processes*, *Physics and Chemistry of the Earth*, Vol. 22, Pergamon Press, London, pp. 653–662.

Green, J. L.: 1988, 'Ray Tracing of Planetary Radio Emissions', in *Planetary Radio Emissions II, Proceedings of the 2nd international workshop*, Graz, Austria, pp. 355–379.

Green, J. L., Fung, S. F. and Burch, J. L.: 1996, 'Application of Magnetospheric Imaging Techniques to Global Substorm Dynamics', *Proceedings of the 3rd International Conference on Substorms,* Versailles, ESA SP-389, 655–661.

Green, J., Fung, S., Gallagher, D., Fok, M.-C., Wilson, G., Gladstone, G., Perez, J., Reiff, P., Burch, J. and Moore, T.: 1998a, 'Global-Scale Imaging: New Approaches in Magnetospheric Research', COSPAR Colloquia Series, Magnetospheric Research with Advanced Techniques, Vol. **9**, Pergamon, London, pp. 41–50.

Green, J. L., Taylor, W. W. L., Fung, S. F., Benson, R. F., Calvert, W., Reinisch, B Gallagher, D. L. and Reiff, P.: 1998b, 'Radio Remote Sensing of Magnetospheric Plasmas, Measurement Techniques for Space Plasmas: Fields', *AGU Monograph* **103**, 193.

Gurnett, D. A. and Shaw, R. R.: 1973, 'Electromagnetic Radiation Trapped in the Magnetosphere Above the Plasma Frequency', *J. Geophys. Res.* **78**, 8136.

Haselgrove, J.: 1955, 'Ray Theory and a New Method for Ray Tracing', London Phys. Soc., Report of Conference on the Physics of the Ionosphere, p. 355.

Higel, B. and de Feraudy, H.: 1977, 'Experimental and Theoretical First Approach to fH Plasma Resonance from a Relaxation Sounding Rocket Experiment', *Radio Sci.* **12**, 879.

Higel, B. and Wu, L.: 1984, 'Electron Density and Plasmapause Characteristics at 6.6 RE. A Statistical Study of the GEOS 2 Relaxation Sounder Data', *J. Geophys. Res.* **89**, 1583.

Ho, D. and Carpenter, D. L.: 1976, 'Outlying Plasmasphere Structure Detected by Whistlers', *Planet. Space Sci.* **24**, 987.

Horne, R. B.: 1995, 'Propagation to the Ground at High Latitudes of Auroral Radio Noise Below the Electron Gyrofrequency', *J. Geophys. Res.* **100**, 14637.

Horwitz, J. L., Comfort, R. H. and Chappell, C. R.: 1990, 'A Statistical Characterization of Plasmasphere Density Structure and Boundary Locations', *J. Geophys. Res.* **95**, 7937.

Huang, X. and Reinisch, B. W.: 1982, 'Automatic Calculation of Electron Density Profiles from Digital Ionograms 2. True Height Inversion of Topside Ionograms with the Profile-Fitting Method', *Radio Sci.* **17**, 837.

Issautier, K., Meyer-Vernet, N., Moncuquet, M. and Hoang, S.: 1999, 'Quasi-Thermal Noise in a Drifting Plasma: Theory and Application to Solar Wind Diagnostic on *Ulysses*', *J. Geophys. Res.* (in press).

Jackson, J. E.: 1969, 'The Reduction of Topside Ionograms to Electron-Density Profiles', *Proc. IEEE* **57**, 960.

Jackson, J. E., Schmerling, E. R. and Whitteker, J. H.: 1980, 'Mini-Review on Topside Sounding', *IEEE Trans. Antennas Propagat.* **AP-28**, 284.

Jackson, J. E.: 1986, 'Alouette-ISIS Program Summary', NSSDC Report 86-09, National Space Science Data Center, Greenbelt, Maryland.

James, H. G.: 1979, 'Wave Propagation Experiments at Medium Frequencies between Two Ionospheric Satellites 3. Z mode pulses', *J. Geophys. Res.* **84**, 499–506.

Kimura, I.: 1966, 'Effects of Ions on Whistler Mode Ray Tracing', *Radio Science 1 (New Series)* **3**, 269.

Koons, H. C.: 1989, 'Observations of Larger-Amplitude, Whistler Mode Wave Ducts in the Outer Plasmasphere', *J. Geophys. Res.* **94**, 15383.

Koons, H. C. and Fennell, J. F.: 1984, 'Fine Structure in Electrostatic Emission Bands between Electron Gyrofrequency Harmonics', *J. Geophys. Res.* **89**, 3015–3018.

Kessel, R. L., Chen, S.-H., Green, J. L., Fung, S. F., Boardsen, S. A., Tan, L. C., Eastman, T. E., Craven, J. D. and Frank, L. A.: 1996, 'Evidence of High-Latitude Reconnection During Northward IMF: Hawkeye Observations', *Geophys. Res. Lett.* **23**, 583.

Kurth, W. S.: 1992, 'Comparative Observations of Plasma Waves at the Outer Planets', *Adv. Space Res.* **12**, (8)83.

LeDocq, M. J., Gurnett, D. A. and Anderson, R. R.: 1994, 'Electron Number Density Fluctuations Near the Plasmapause Observed by CRRES Spacecraft', *J. Geophys. Res.* **99**, 23661.

LeSager, P., Canu P. and Cornilleau-Wehrlin, N.: 1998, 'Impact of the *Ulysses* Velocity on the Diagnosis of the Electron Density by the Unified Radio and Plasma Wave Sounder in the Outskirts of the Io Torus', *J. Geophys. Res.* **103**, 26,667.

Lemaire, J.: 1975, 'The Mechanisms of Formation of the Plasmapause', *Annales de Geophysique* **31**, 175.

Lemaire, J. and Gringauz, K. I.: 1998, The Earth's Plasmasphere, Cambridge University Press.

Lennartson, W. and Reasoner, D. C.: 1978, 'Low Energy Plasma Observations at Synchronous Orbit', *J. Geophys. Res.* **83**, 2145.

Lockwood, G. E. K.: 1973, 'Side Band and Harmonic Radiation from Topside Sounders', *J. Geophys. Res.* **78**, 2244.

Lund, E. J., Labelle, J. and Treumann, R. A.: 1995, 'On Quasi-Thermal Noise Fluctuations Near the Plasma Frequency on the Outer Plasmasphere: a Case Study', *J. Geophys. Res.* **99**, 23651.

Matsumoto, H. and Usui, H.: 1997, 'Intense Bursts of Electron Cyclotron Harmonic Waves near the Dayside Magnetopause Observed by GEOTAIL', *Geophys. Res. Lett.* **24**, 49.

Meyer-Vernet, N. and Perche, C.: 1989, 'Toolkit for Antennae and Thermal Noise Near the Plasma Frequency', *J. Geophys. Res.* **94**, 2405.

Meyer-Vernet, N., Hoang S. and Moncuquet, M.: 1993, 'Bernstein Waves in the Io Torus: a Novel Kind of Electron Temperature Sensor', *J. Geophys. Res.* **98**, 21163.

Meyer-Vernet, N., Moncuquet, M. and Hoang, S.: 1995, 'Temperature Inversion in the Io Plasma Torus', *Icarus* **116**, 202.

Meyer-Vernet, N., Hoang, S., Issautier, K., Maksimovic, M., Manning, R., Moncuquet, M. and Stone, R.: 1998, 'Measuring Plasma Parameters with Thermal Noise Spectroscopy', in E. Borovsky and R. Pfaff (eds), *Geophysical Monograph 103: Measurements Techniques in Space Plasmas*, pp. 205–210.

Moncuquet, M., Meyer-Vernet, N., Bougeret, J.-L., Manning, R., Perche, C. and Kaiser, M. L.: 1995, 'Wind Passes through the Outer Plasmasphere: Plasma Diagnosis from the Quasi-Thermal Noise Spectrum Measured by the Waves Experiment', *Suppl. Eos* **76**, 17, S221.

Moncuquet, M., Meyer-Vernet, N., Hoang, S., Forsyth, R. J. and Canu, P.: 1997, 'Detection of Bernstein Wave Forbidden Bands: a New Day to Measure the Electron Density', *J. Geophys. Res.* **102**, 2373.

Moldwin, M. B., Thomsen, M. G., Bame, S. J., McComas, D. J. and Moore, K. R.: 1994, 'An Examination of the Structure and Dynamics of the Outer Plasmasphere Using Multiple Geosynchronous Satellites', *J. Geophys. Res.* **99**, 11475.

Moldwin, M. B., Thomsen, M. F., Bame, S. J., McComas, D. and Reeves, G. D.: 1995, 'The Fine-Scale Structure of the Outer Plasmasphere', *J. Geophys. Res.* **100**, 9649.

Newell, P. T.: 1995, 'Do the Dayside Cusps Blink?', *Rev. Geophys. Suppl.*, U.S. national Report to IUGG, 665.

Ober, D. M., Horwitz, J. L. and Gallagher, D. L.: 1997, 'Formation of Density Troughs Embedded in the Outer Plasmasphere by Subauroral Ion Drifts (SAID)', *J. Geophys. Res.* **102**, 14595.

Osherovich, V. A., Benson, R. F., Fainberg, J., Stone R. G. and MacDowall, R. J.: 1993a, 'Sounder Stimulated Dn Resonances in Jupiter's Io Plasma Torus', *J. Geophys. Res.* **98**, 18751.

Osherovich, V. A., Farrugia, C. J., Burlaga, L. F., Lepping, R. P., Fainberg, J. and Stone, R. G.: 1993b, 'Polytropic Relationship in Interplanetary Magnetic Clouds', *J. Geophys. Res.* **98**, 15,331.

Oya, H.: 1972, 'Turbulence of Electrostatic Electron Cyclotron Harmonic Waves Observed by Ogo 5', *J. Geophys. Res.* **77**, 3483.

Oya, H. and Ono, T.: 1987, 'Stimulation of Plasma Waves in the Magnetosphere Using Satellite JIKIKEN (EXOS B) Part II: Plasma Density Across the Plasmapause', *J. Geomag. Geoelectr.* **39**, 591.

Park, C. G. and Carpenter, D. L.: 1970, 'Whistler Evidence of Large-Scale Electron-Density Irregularities in the Plasmasphere', *J. Geophys. Res.* **75**, 3825.

Pierrard, V. and Lemaire, J.: 1996, 'Lorentzian Ion Exosphere Model', *J. Geophys. Res.* **101**, 7923.

Potemra, T. A., Erlandson, R. E., Zanetti, L. J., Arnoldy, R. L., Woch, J. and Friis-Christensen, E.: 1992, 'The Dynamic Cusp', *J. Geophys. Res.* **97**, 2835.

Reiff, P. H., Green, J. L., Benson, R. F., Carpenter, D. L., Calvert, W., Fung, S. F., Gallagher, D. L., Omura, Y., Reinisch, B. W., Smith, M. F. and Taylor, W. W. L.: 1994, 'Remote Sensing of Substorm Dynamics via Radio Sounding, Substorms 2', in J. R. Kan, J. D. Craven and S.-I. Akasofu (eds.), *Proceedings of the Second International Conference on Substorms,* University of Alaska Press, Fairbanks, Alaska, pp. 281–287.

Reiff, P.H., Boyle, C. B., Green, J. L., Fung, S. F., Benson, R. F., Calvert, W. and Taylor, W. W. L.: 1996, 'Radio Sounding of Multiscale Plasmas', in T. Chang and J. R. Jasperse (eds.), *Physics of Space Plasmas, 14*, MIT Press, Cambridge, MA, pp. 415–429.

Reinisch, B. W., Sales, G. S., Haines, D. M., Fung, S. F. and Taylor, W. W. L.: 1999, 'Radio Wave Active Doppler Imaging of Space Plasma Structures: Angle-of-Arrival, Wave Polarization, and Faraday Rotation Measurements with RPI', *Radio Sci.* **34**, 1513–1524.

Reinisch, B. W., Haines, D. M., Bibl, K., Cheney, G., Galkin , I. A., Huang, X., Myers, S. H., Sales, G. S., Benson, R. F., Fung, S. F., Green, J. L., Taylor, W.W.L., Bougeret, J.-L., Manning, R., Meyer-Vernet, N., Moncuquet, M., Carpenter, D. L., Gallagher, D. L. and Reiff, P.: 2000, 'The Radio Plasma Imager Investigation on the IMAGE Spacecraft', *Space Sci. Rev.* **91**, 319–359 (this issue).

Roelof, E. C. and Sibeck, D. G.: 1993, 'Magnetopause Shape as a Bivariate Function of Interplanetary Magnetic Field Bz and Solar Wind Dynamic Pressure', *J. Geophys. Res.* **98**, 21421.

Scudder, J. D.: 1992, 'On the Causes of Temperature Change in Inhomogeneous Low-Density Astrophysical Plasmas', *Astrophys. J.* **398**, 299.

Spiro, R. W., Harel, M., Wolf, R. A. and Reiff, P. H.: 1981, 'Quantitative Simulation of a Magnetospheric Substorm, 3. Plasmaspheric Electric Fields and Evolution of the Plasmapause', *J. Geophys. Res.* **86**, 2261.

Stix, T. H.: 1962, *The Theory of Plasma Waves*, McGraw-Hill, New York, p. 27.

Taylor, H. A., Jr., Grebowsky, J. M. and Walsh, W. J.: 1970, 'Structured Variations of the Plasmapause: Evidence of a Corotating Plasma Tail', *J. Geophys. Res.* **76**, 6806.

Warren, E. S.: 1969, 'The Topside Ionosphere During Geomagnetic Storms', *Proc. IEEE* **57**, 1029.

Weiss, L. A., Lambour, R. L., Elphic, R. C. and Thomsen, M. F.: 1997, 'Study of Plasmaspheric Evolution Using Geosynchronous Observations and Global Modeling', *Geophys. Res. Lett.* **24**, 599.

Yamauchi, M., Lundin, R. and Potemra, T. A.: 1995, 'Dynamic Response of the Cusp Morphology to the Interplanetary Magnetic Field Changes: an Example Observed by Viking', *J. Geophys. Res.* **100**, 7661.

Xue, S., Reiff, P. H. and Onsager, T.: 1997, 'Cusp Ion Injection and Number Density Modeling in Realistic Electric and Magnetic Fields', *Phys. Chem. Earth* **22**, 735.